HHS Public Access

Author manuscript

Cell Rep. Author manuscript; available in PMC 2023 July 28.

Published in final edited form as:

Cell Rep. 2022 May 31; 39(9): 110876. doi:10.1016/j.celrep.2022.110876.

A humanized β_2 integrin knockin mouse reveals localized intra- and extravascular neutrophil integrin activation *in vivo*

Lai Wen[1], **Alex Marki**[1], **Zhihao Wang**[1], **Marco Orecchioni**[1], **Jeffrey Makings**[1], **Monica Billitti**[1], **Erpei Wang**[1], **Sujit S.A. Suthahar**[1], **Kenneth Kim**[2], **William B. Kiosses**[3], **Zbigniew Mikulski**[3], **Klaus Ley**[1,4,5,*]

[1]Center for Autoimmunity and Inflammation, La Jolla Institute for Immunology, 9420 Athena Circle, La Jolla, CA 92037, USA

[2]Histopathology Core Facility, La Jolla Institute for Immunology, 9420 Athena Circle, La Jolla, CA 92037, USA

[3]Microscopy and Histology Core Facility, La Jolla Institute for Immunology, 9420 Athena Circle, La Jolla, CA 92037, USA

[4]Department of Bioengineering, University of California, San Diego, 9500 Gilman Drive, La Jolla, CA 92093, USA

[5]Lead contact

SUMMARY

β_2 integrins are leukocyte-specific adhesion molecules that are essential for leukocyte recruitment. The lack of tools for reporting β_2 integrin activation in mice hindered the study of β_2 integrin-related immune responses *in vivo*. Here, we generated a humanized β_2 integrin knockin mouse strain by targeting the human β_2 integrin coding sequence into the mouse *Itgb2* locus to enable imaging of β_2 integrin activation using the KIM127 (extension) and mAb24 (high-affinity) reporter antibodies. Using a CXCL1-induced acute inflammation model, we show the local dynamics of β_2 integrin activation in arresting neutrophils *in vivo* in venules of the mouse cremaster muscle. Activated integrins are highly concentrated in a small area at the rear of arresting neutrophils *in vivo*. In a high-dose lipopolysaccharide model, we find that β_2 integrins are activated in association with elevated neutrophil adhesion in lung and liver. Thus, these mice enable studies of β_2 integrin activation *in vivo*.

*Correspondence: klaus@lji.org.

AUTHOR CONTRIBUTIONS

L.W. and K.L. designed experiments. L.W. performed most experiments and data analysis. A.M. and L.W. performed intravital imaging. Z.W., M.O., and J.M. helped with FACS experiments and the LPS model. Z.W., J.M., M.B., and E.W. helped with mouse husbandry. S.S.A.S. helped with data analysis. W.B.K. and Z.M. provided microscopy expertise. K.K. performed histopathology analysis. K.L. supervised the project and provided funding. K.L. and L.W. wrote the manuscript. All authors read and provided comments on the manuscript.

SUPPLEMENTAL INFORMATION

Supplemental information can be found online at https://doi.org/10.1016/j.celrep.2022.110876.

DECLARATION OF INTERESTS

The authors declare no competing interests.

In brief

Wen et al. generated a reporter mouse for analysis of leukocyte β_2 integrin activation *in vivo* and show the dynamics and subcellular localization of β_2 integrin activation during neutrophil adhesion and transendothelial migration. This mouse also allows analysis of β_2 integrin activation in disease models.

Graphical Abstract

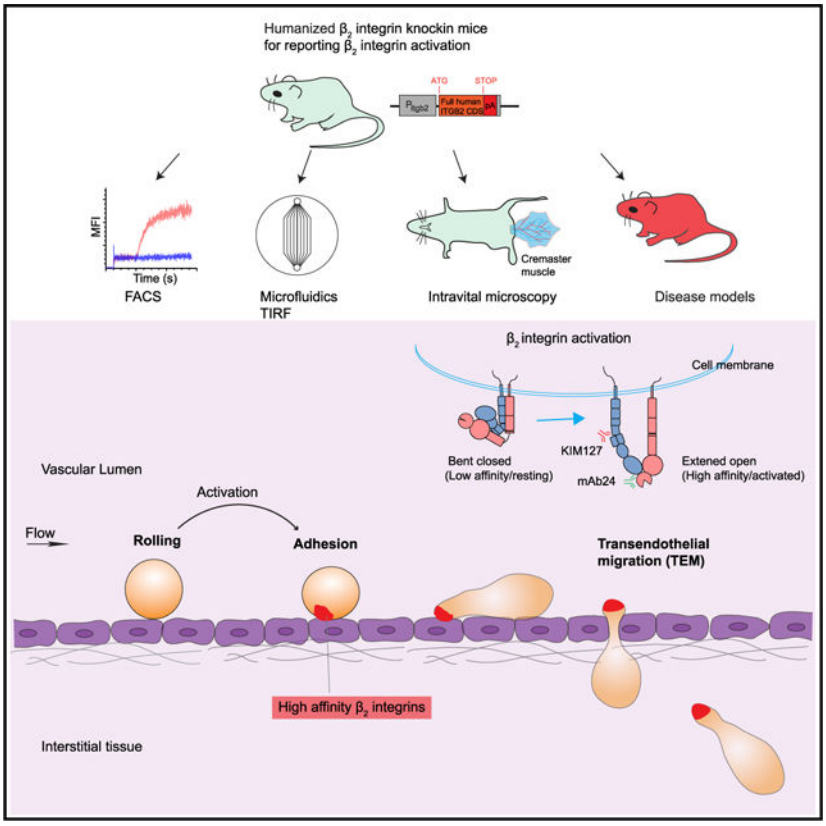

INTRODUCTION

β_2 integrins are expressed in all leukocyte types (e.g., neutrophils, lymphocytes, monocytes) and are essential for leukocyte recruitment as well as for other immunological processes such as phagocytosis, reactive oxygen species production, and T cell activation (Scharffetter-Kochanek et al., 1998). Mutations in the *ITGB2* gene coding for the β_2 integrin subunit (also known as CD18) lead to defective adhesion and the subsequent migration into inflamed areas. Patients with this defect develop leukocyte adhesion deficiency type I (LAD-I) syndrome characterized by immunodeficiency resulting in recurrent infections (Anderson and Springer, 1987).

In blood leukocytes, β_2 integrins are in a resting (inactive) state with low affinity for their ligands; they quickly switch to an activated, high-affinity state in response to inflammatory

signals. This process is known as integrin inside-out activation (Hynes, 2002; Ley et al., 2018; Shattil et al., 2010; Springer and Dustin, 2012; Wen et al., 2022). In general, integrin activation controls cell adhesion. Such control is particularly important in the vasculature, where dynamic blood flow physically opposes cell attachment. Circulating leukocytes including neutrophils arrest on activated endothelium in response to inflammatory signals using β_2 integrins (Kolaczkowska and Kubes, 2013; Ley et al., 2007).

Integrins are known to exist in distinct activation states, which exhibit different affinities for ligand. Resting integrins adopt a bent conformation with low affinity for ligand. Upon exposure to chemokines such as interleukin-8 (IL-8), integrins undergo dramatic conformational changes that are associated with activation. The main changes are extension (standing up, E^+) and opening of the αI domain (high affinity, H^+). The E^+ and H^+ conformations of human β_2 integrin can be recognized by two activation-specific monoclonal antibodies (mAbs), KIM127 and mAb24. KIM127 binds an epitope hidden in the knee of bent β_2 and thus reports E^+. mAb24 binds an epitope in the β_2 I-like domain that is induced when the αI domain is activated, thus reporting H^+ (Dransfield and Hogg, 1989; Robinson et al., 1992).

β_2 integrins have four known conformations: bent (E^-H^-) with no known adhesive function, extended low affinity (E^+H^-) that may slow down rolling cells (Lefort et al., 2012), bent high affinity (E^-H^+), and extended high affinity (E^+H^+). E^-H^+ β_2 integrins bind small-molecule ligands (Gupta et al., 2007) and neutrophil cell surface ligands such as intracellular adhesion molecule 1 (ICAM-1) and ICAM-3 in *cis* (Fan et al., 2016, 2019), effectively inhibiting adhesion. E^+H^+ β_2 integrins have up to 10,000-fold higher affinity than E^-H^- (Shimaoka et al., 2003), bind ligands such as ICAMs in *trans*, and induce arrest from rolling under shear stress (Fan et al., 2016).

The activation status of β_2 integrins *in vivo* is unknown, as are the dynamics of their activation. The lack of a β_2 integrin activation reporter mouse has hampered the study of β_2 integrin activation signaling. It is unknown how rapidly β_2 integrins become activated, how long they stay activated *in vivo*, and which of the three activated states dominate during arrest, transmigration, migration in the tissue, phagocytosis, and other *in vivo* functions. Here, we generated a humanized β_2 integrin knockin mouse that enables dissection of integrin activation conformations, kinetics, and locations *in vivo*.

Attempts to produce activation reporter antibodies for mouse β_2 have remained unsuccessful. KIM127 and mAb24 only report human β_2 integrin activation-specific epitopes and do not bind mouse integrins. It is known that the mouse integrin α subunits of LFA-1 (αL), Mac-1 (αM), and CD11c/CD18 (αX) pair with human β_2 in granulocytes and other hematopoietic cells *in vitro* (Krauss et al., 1991). Human β_2 is necessary and sufficient for the expression of intact, functional β_2 integrins on the cell surface in vitro. To study β_2 integrin activation *in vivo*, we targeted the human β_2 coding sequence into the mouse β_2 locus, generating a humanized β_2 integrin knockin mouse. This mouse is knockout for mouse β_2. The human

β_2 is expressed in the natural locus with all promoters and enhancers intact, thus enabling physiologic expression in all leukocytes.

RESULTS

Generation and characterization of β_2 integrin activation reporter mice

To enable the analysis of integrin activation-specific epitopes in primary mouse neutrophils, we generated a humanized β_2 knockin (hITGB2 KI) mouse, in which human instead of mouse integrin β_2 is expressed (Figure 1). A gene cassette coding for the cDNA of human *ITGB2* was inserted in frame with the first coding ATG in exon 2 of the *Itgb2* locus. The neomycin cassette used for selection was excised by Flp recombinase. The resulting knockin transgene is under the control of the endogenous *Itgb2* promoter, ensuring a natural expression pattern. The homozygous hITGB2 KI mice are born at Mendelian frequencies, are apparently healthy, gain weight at the same rate as wild-type (WT) mice, and have a normal life expectancy. Unlike *Itgb2* knockout mice (Scharffetter-Kochanek et al., 1998), hITGB2 KI mice do not have LAD-I symptoms.

First, we established that KIM127 (E^+) and mAb24 (H^+) can indeed report β_2 integrin activation in hITGB2 KI mouse neutrophils. As a positive control, we confirmed that mAb24 binding was sharply increased after adding IL-8 (100 ng/mL) to human whole blood in a flow-cytometric homogeneous binding assay (Chigaev et al., 2009) gated for neutrophils by CD66b, reaching a plateau after ~100 s. KIM127 binding was also significantly increased and continued to increase for at least 400 s (Figure 2A). Next, we measured binding of mAb24 and KIM127 in ITGB2 KI mouse whole blood using the same flow-cytometric homogeneous binding assay gated for neutrophils by Ly6G (Figure 2B). Real-time measurement of β_2 integrin activation using the reporter antibody binding assay showed that the CXCR2 ligand CXCL1 (at 10 ng/mL) induced significant increases of mAb24 (Figure 2B, upper panel) and KIM127 (Figure 2B, lower panel) in neutrophils from hITGB2 KI mice with patterns similar to human neutrophils. As expected, we saw no reactivity for mAb24 or KIM127 in WT mouse neutrophils (Figure 2C).

Mouse neutrophil arrest and activated β_2 integrins with E^+H^+ conformation

In vitro studies with human neutrophils rolling on substrates of selectins and ICAM-1 (Fan et al., 2016; Yago et al., 2018) or on endothelial cells (Morikis et al., 2017) showed that arrest from rolling is associated with β_2 integrin activation. The best maps of activated integrins (Fan etal., 2016) were generated by quantitative dynamic footprinting (qDF) (Sundd et al., 2010; Wen et al., 2020), a method based on variable angle total internal reflection (TIRF) microscopy. Because the activation reporter antibodies work only for human and not for mouse integrins, all published data are for human neutrophils, lymphocytes, or cell lines. To test whether integrin activation during arrest was similar in mouse neutrophils, we used qDF to map KIM127 (E^+) and mAb24 (H^+) binding dynamics during hITGB2 KI mouse neutrophil arrest from rolling in response to CXCL1 (Figure 3A). We labeled neutrophils with an anti-Ly6G anti-body. Ly6G is neutrophil specific, abundantly expressed, and clearly shows the microvilli by qDF. Neutrophils were perfused at 6 dyn/cm^2

wall shear stress through a microfluidic flow chamber coated with recombinant mouse P-selectin-Fc and ICAM-1-Fc. We then infused 10 ng/mL CXCL1 to rolling neutrophils. During rolling, some E^+ integrins were present on the surface of mouse neutrophils, and a few transient patches of H^+ integrins were also observed (Video S1). However, a significant increase of E^+H^+ ($KIM127^+mAb24^+$) integrins was not seen until the time of arrest at t = 0 s (Figures 3B and 3C). This is in line with previous studies on human neutrophils (Fan et al., 2016). As few as 2 ± 1 clusters of E^+H^+ ($KIM127^+mAb24^+$) integrins were needed for neutrophil arrest (Figure 3). $KIM127^+$ and $mAb24^+$ clusters also increased in size after arrest. The most dramatic increase was observed in the size of the E^+H^+ clusters, suggesting that neutrophils arrest when sufficient patches of extended high-affinity β_2 integrins form. Both KIM127 and mAb24 binding continued to increase after arrest (Figure 3B). The presence of E^-H^+ integrin clusters on the surface of mouse neutrophils supports the recent discovery of the non-canonical integrin activation pathway, where the high-affinity (H^+) conformation is acquired before extension (Fan et al., 2016).

Local integrin activation in arresting and migrating neutrophils *in vivo*

Side-view images of arresting neutrophils with reporter antibodies for integrin activation have not been reported. Intravital microscopy readily yields side-view images of rolling and arresting neutrophils, and hITGB2 KI mice now allow monitoring of the integrin activation status. Integrin dynamics during arrest *in vivo* have not been reported in any system. To investigate mAb24 and KIM127 binding epitope expression in response to CXCL1 stimulation in mouse neutrophils *in vivo*, we performed intravital imaging of mouse neutrophil arrest in the microcirculation of mouse cremaster muscle venules (Figure 4). Both antibodies were injected into the mice 3–5 min prior to imaging. mAb24 and KIM127 binding was rarely detected in rolling neutrophils in the bloodstream. During an observation period of 5 min, out of 102 cells observed, 7 cells (less than 7%) displayed KIM127 binding (E^+H^-) integrin (Figures 4A and S1A–S1D; Video S2). Only one cell showed E^+H^+ β_2 integrins (Figure S1B). Occasionally, we observed spontaneous neutrophil adhesion with E^+H^+ integrin activation (Figure S1C). Upon injection of 300 ng of CXCL1 into hITGB2 KI mice through a carotid cannula, blood neutrophils started significantly binding mAb24 and KIM127 (Figures 4A–4C). This binding was not observed at the time of arrest, because, unlike qDF microscopy used in Figure 3, confocal microscopy is not sensitive enough to pick up the small signal of a few clusters at arrest. However, KIM127 and mAb24 signal appeared during the next ~60 s. All images and data of adherent neutrophils shown in Figure 4 were obtained at ~60 s after arrest.

In all arrested neutrophils, there was little KIM127 and mAb24 signal on top of the cell, the side facing the vessel axis, or the front, the side facing in the direction of flow. KIM127 and mAb24 signal increased steadily along the bottom of each neutrophil, the side facing the endothelium, and reached the highest intensities at the rear, the side facing against the direction of flow (Figures 4B and 4D). These local high-affinity integrins become visible at 1 min and maximal at around 2 min after arrest. Due to the local distribution of activated integrin and the position of the neutrophils in the vessel, not all neutrophils show mAb24

and KIM127 signals in the focal plane of the same image. Often we could observe activated integrins by changing the focal plane using a different frame of the recordings (Figure S2). All arrested neutrophils showed similar integrin activation profiles. E^-H^+ ($mAb24^+KIM127^-$) β_2 integrin clusters bind ligand in cis and do not contribute to adhesion (Fan et al., 2016). $mAb24^-KIM127^-$ clusters contribute to slow rolling but do not trigger arrest (Kuwano et al., 2010; Lefort et al., 2012). Fully active E^+H^+ β_2 integrins must bind both KIM127 and mAb24, and only E^+H^+ molecules can stably bind ligand in *trans* and cause arrest. We estimated the presence of E^+H^+ integrins by calculating the product of mAb24 and KIM127 signal (Figures 4D and 4F). The product of $mAb24^-KIM127^+$ pixels is zero, as is the product of $mAb24^+KIM127^-$ pixels. Only $mAb24^+KIM127^+$ pixels (extended and high affinity) can contribute to arrest, and their product is finite (not zero). In each neutrophil, this product reached a clear maximum at the bottom rear, the corner between the endothelium and the free neutrophil membrane where peeling forces are maximal (Damiano et al., 1996; Dembo et al., 1988; Pospieszalska et al., 2011; Tozeren and Ley, 1992). Some neutrophils showed a secondary maximum under the neutrophil, suggesting that these cells would have a second "sticky patch" if the first one had not successfully induced arrest (Figure S3). Since *in vivo* imaging of integrin activation in arresting cells *in vivo* has not been possible previously, there are no other data with which to compare our findings.

Next, we analyzed KIM127 and mAb24 intensity around the circumference of eight neutrophils. To average the signals, mAb24, KIM127, and the product KIM127 × mAb24 each were normalized to 1 for the average. The data were distributed into 40 bins, and the mean ± range for each bin as well as the significance for being different from 1 were calculated (Figure 4F). To further visualize the dynamics of integrin activation *in vivo*, we performed time- and space-resolved confocal imaging of mouse neutrophil arrest in the mouse microcirculation of the mouse cremaster muscle. Three-dimensional reconstruction of the imaging in real time further confirmed the localized distribution of activated β_2 integrins (Video S3).

Although a great deal has been learned about β_2 integrins in mediating the early steps in leukocyte adhesion cascade, including rolling and firm adhesion, little is known about the dynamic and spatial regulation of integrin activation during leukocyte transmigration. We used glass micropipettes to inject 10 μM *N*-formylmethionyl-leucyl-phenylalanine (fMLP) locally into cremaster muscle to induce neutrophil transmigration. mAb24 and KIM127 were injected through the carotid artery cannula. We visualized the mAb24 and KIM127 binding in migrating neutrophils. Interestingly, both $mAb24^+$ and $KIM127^+$ integrins were concentrated at the rear of migrating neutrophils throughout the process of extravasation to interstitial migration (Figure S4 and Videos S4–S6). We conclude that high-affinity β_2 integrins are located at the uropod of neutrophils during and after transendothelial migration.

Human integrin β_2 (CD18) is expressed in the major mouse leukocyte populations in hITGB2 KI mice

Although we made the hITGB2 KI mouse to study neutrophil arrest, we tested whether the hITGB2 KI mouse would be useful for studying other leukocytes. We examined the expression of CD18 (the β_2 subunit) in other immune cell types: classical monocytes, non-classical monocytes, CD4 and CD8 T cells, B cells, and natural killer cells. Two antibodies, one against human CD18 (β_2) (clone TS1/18) and one against mouse CD18 (clone GAME-46), were used to test the CD18 expression in whole mouse blood by flow cytometry. By gating on various immune cell types (see Figure S5 for gating scheme), we confirmed that human CD18 expression was only detected in hITGB2 mice, and only mouse CD18 was detected in WT mice (Figure 5A), on all leukocyte types tested. This indicates that the human CD18 is faithfully expressed under the control of the endogenous CD18 promoter as expected.

This approach does not allow for quantitative comparison of expression, because staining with two different antibodies labeled with two different fluorochromes does not yield comparable intensities. Therefore, to compare the expression levels of mouse α and human β_2 integrins in hITGB2 KI mice with mouse αβ in WT mice, we measured the three expressed α subunits (CD11a or αL, CD11b or αM, and CD11c or αX). Since the α chains are all mouse, we were able to use the same mAbs for WT and hITGB2 KI mice. This approach provides a direct comparison and an indirect estimate of β_2 expression by comparing α subunit expression between WT and hITGB2 KI mice. The antibody staining analyzed by fluorescence-activated cell sorting (FACS) shows that the expression of CD11a, CD11b, and CD11c was similar in hITGB2 KI mice compared with WT mice (Figure 5B).

β_2 integrins are activated in neutrophils of LPS-treated mice

To study β_2 integrin activation under pathologic conditions, we intraperitoneally injected mice with 40 mg/kg lipopolysaccharide (LPS) (Marki et al., 2021) and examined neutrophil trafficking and integrin activation in this model. The migration of neutrophils from the intravascular to the extravascular compartment is initiated by the “margination” or movement of the neutrophils from central stream to the periphery of a vessel through rolling and adhesion to the postcapillary endothelium (Alves-Filho et al., 2010). Indeed, we observed a dramatic increase of neutrophil margination along vessels of LPS-treated mouse lungs using hematoxylin and eosin (H&E) stain (Figure 6A). In pulmonary blood vessels in control mice, few nucleated cells were seen within proximity of the endothelial walls (Figure 6A, left). In LPS-treated mice, numerous nucleated cells were seen abutting the endothelial walls with many cells showing neutrophil morphology (Figure 6A, right). In control mouse livers, few neutrophils were seen (Figure 6B, left) compared with LPS mice in which there were numerous neutrophils within sinusoids (Figure 6B, right).

We then used flow cytometry to measure intravascular neutrophils in lung and liver by labeling the intravascular neutrophils with intravenous injection of an anti-CD45 antibody 3 min prior to harvesting the mice (Galkina et al., 2005). In this short incubation time the antibody is retained in the circulation and does not label the extravasated neutrophils.

LPS resulted in elevated intravascular neutrophils in the lung and liver (Figure 6C). FACS analysis showed that most neutrophils (50%–60% of live cells) in the lung and liver remain intravascular in this model (Figure 6C). Knockin mice were functionally similar to WT mice in inducing neutrophil recruitment (Figure 6C).

To address integrin activation in whole blood of LPS-treated hITGB2 KI mice, we stained it with mAb24 and KIM127. LPS treatment resulted in widespread >20-fold induction of KIM127 and mAb24 double-positive (E^+H^+) neutrophils at 6 h after LPS treatment (Figures 6D and 6E). LPS also resulted in a ~3-fold increase of neutrophil numbers in the blood (Figures 6F and 6G), indicating that under these conditions a large number of neutrophils are mobilized from the bone marrow into the peripheral blood. The percentages of neutrophils were significantly increased in both lung and liver in LPS-treated mice (Figure S6). Exacerbated neutrophil β_2 integrin activation and β_2 integrin-mediated neutrophil recruitment may lead to deleterious effects on organ function during this lethal LPS model.

DISCUSSION

β_2 integrins are expressed in all leukocyte types. We describe the development of a mouse model that allows for analysis of mouse β_2 integrin activation in all leukocytes *in vivo*. We studied the spatiotemporal dynamics of β_2 integrin activation in neutrophils using time-resolved flow cytometry, qDF imaging, and intravital imaging. We show side-view images of integrin activation during neutrophil arrest. Activated integrins in arresting neutrophils *in vivo* are highly localized and mainly distributed at the interface of neutrophils and the endothelium at the rear side of neutrophils facing against the blood flow. In a lethal LPS model, we show massive integrin activation on neutrophils in peripheral blood. Neutrophils are deposited along the vessels of lungs and infiltrate the livers.

Integrin activation can occur through the canonical pathway of conformational transition from bent (E^-H^-) to extended (E^+H^-) to fully activated (E^+H^+). Recent work identified an alternative pathway where the headpiece opens (H^+) before the integrin extends (E^-) during arrest of primary human neutrophils. E^-H^+ integrins bind to their ligand ICAMs (ICAM-1 and −3 for human, ICAM-1 and −2 for mouse) in *cis* (on the same cell), implicating an autoinhibitory role of E^-H^+ integrins in neutrophil activation. It was not known previously whether E^-H^+ β_2 integrins existed *in vivo*. Here, we show that E^-H^+ integrins are abundant in mouse primary neutrophils as qDF imaging shows single positive activated integrins ($mAb24^+KIM127^-$), which corresponds to the E^-H^+ conformation. Thus, β_2 integrin extension and high affinity can be uncoupled. This demonstrates that the alternative integrin activation pathway exists in mouse neutrophils *in vivo*.

Fewer clusters were needed for mouse neutrophil arrest than were required for human neutrophil arrest at the same wall shear stress (Fan et al., 2016). In part, the reason might be the different drag force exerted on arresting neutrophils. Mouse and human neutrophils have a diameter of ~7 μm (Marki et al., 2016) and 8.4 μm (Downey et al., 1990), respectively.

This correlates with lower drag forces on the smaller mouse neutrophils (942 pN and 1,357 pN acting at 6 dyn/cm^2 on mouse and human neutrophils, respectively).

It has long been recognized that integrins are mechanoreceptors, and integrin-mediated adhesions are intrinsically mechanosensitive. Initially, we were surprised that the integrin activation is locally distributed at the rear of arresting mouse neutrophils, facing against the blood flow, although the chemokine CXCL1 is globally applied through the carotid catheter. Our experiments showed that the E^+H^+ integrins reached a clear maximum at the bottom rear, the corner between the endothelium and the free neutrophil membrane where peeling forces are maximal (Damiano et al., 1996; Dembo et al., 1988; Pospieszalska et al., 2011; Tozeren and Ley, 1992). This suggests that the local integrin activation may be a result of integrin-ligand binding in response to shear stress elicited by blood flow. There are no published *in vivo* data on β_2 integrin activation with which we could compare our findings.

We noticed a significant difference in the dynamics of KIM127 epitope expression in mouse neutrophils *in vitro* and *in vivo*. No mAb24 and KIM127 binding was detected in rolling neutrophils in the bloodstream *in vivo*. This suggests that the “creep” seen in KIM127 binding to human neutrophils in flow chambers (Kuwano et al., 2010) may be specific to human neutrophils or to the *in vitro* environment, or both. Perhaps the blood plasma contains or the endothelial cells secrete anti-inflammatory mediators that keep β_2 integrin extension at bay. Consistent with this interpretation, we clearly saw KIM127 “creep” on hITGB2 mouse neutrophils prior to chemokine injection *in vitro* (Figure 3). However, *in vivo* we saw no KIM127 binding prior to neutrophil arrest.

β_2 integrin activation is involved in many immune functions, including formation of inflammatory synapses formed at the interface of neutrophils and endothelium (Simonetal.,2009), leukocyte slow rolling (Kunkel et al., 2000; Zarbock et al., 2007), leukocyte transmigration (Nourshargh and Alon, 2014), and microparticle generation during leukocyte transmigration (Hyun et al., 2012). β_2 integrins participate in the formation of immunological synapses between T cells and antigen-presenting cells (Springer and Dustin, 2012). It has been shown that LFA-1 and ICAM-1 interaction increases the sensitivity of T cells to antigen by 100-fold (Bachmann et al., 1997). β_2 integrins modulate actin dynamics at the immunological synapse (Jankowska et al., 2018). The relative roles of β_2 integrin conformational changes and lateral organization remain largely unknown. Chemokine- or cytokine-induced integrin activation (Alonand Shulman,2011; Bouaouina etal., 2004), duration of integrin activation, role of endothelium in leukocyte activation, and failure of leukocyte arrest (Smith et al., 2006) are areas of great interest involving β_2 integrins.

Changes in neutrophil functions are directly related to sepsis-related morbidity and mortality (Danikas et al., 2008; Muller Kobold et al., 2000). Patients with LAD-I present recurrent bacterial infections that can develop into sepsis (Fagerholm et al., 2019). The severity of the disease varies in relation to the functionality of the β_2 integrin (van de Vijver et al., 2012). LAD-I patients with lower β_2 integrin expression show more severe symptoms and are more likely to develop sepsis. Ligand-specific partial blocking of Mac-1 has recently been shown to protect against bacterial sepsis, while blocking all Mac-1 functions potentiates the severity

of sepsis, indicating the complicated role of β_2 integrins (Wolf et al., 2018). Exacerbated neutrophil activation contributes to tissue damage and the development of organ dysfunction during sepsis. Sepsis is known to be associated with increased neutrophil counts in blood (Sonego et al., 2016). Our findings show that neutrophil β_2 integrins are significantly activated in response to LPS stimulation. At 6 h after LPS, neutrophils accumulate along the blood vessel walls in lungs. These neutrophils stay intravascular. Meanwhile, some neutrophils traffic to the liver extravascular space.

In conclusion, we report the first *in vivo* data on β_2 integrin activation. The hITGB2 KI mouse is a useful tool for studying β_2 integrin activation *in vivo*. This mouse can be crossed with knockout, knockin, or transgenic mice to study specific questions in neutrophils and other leukocyte types under normal and pathologic conditions, or during pharmacotherapy with integrin-blocking or integrin-activating drugs (Ley et al., 2016; Maiguel et al., 2011).

Limitations of the study

One challenge is that the detection of integrin activation reported by conformation-specific reporter antibodies *in vivo* is inherently limited by the detection sensitivity and tissue penetration of intravital imaging. This can be partially overcome by using advanced microscopy such as multiphoton microscopy (Koltsova et al., 2012; McArdle et al., 2019; Pittet and Weissleder, 2011), which has deeper tissue penetration. Intravital microscopy provides top, bottom, and side views of arresting neutrophils, but does not allow for TIRF imaging. Thus, intravital imaging is paired with microfluidics-based TIRF-qDF to reveal the exact location of activated integrins (Wen et al., 2020).

STAR★METHODS

RESOURCE AVAILABILITY

Lead contact—Further information and requests for resources and reagents should be directed to and will be fulfilled by the lead contact, Klaus Ley (klaus@lji.org).

Materials availability—Mouse lines generated in this study are available upon request and payment of a nominal fee to cover breeding, genotyping, boxing, and shipping.

Data and code availability

- All data supporting the findings of this study are available within the paper and its supplemental information files.
- This study did not generate or analyze unique datasets or code.
- Any additional information required to reanalyze the data reported in this paper is available from the lead contact upon request.

EXPERIMENTAL MODEL AND SUBJECT DETAILS

Human neutrophils—Heparinized whole blood was obtained from healthy human donors (females or males from 20–40 years old) after informed consent, as approved by the

Institutional Review Board of the La Jolla Institute of Immunology in accordance with the Declaration of Helsinki. Informed consent was obtained from all donors.

Mice—WT (C57BL/6J) mice (6–8 weeks old females or males) were purchased from the Jackson Laboratory. Mice were handled according to guidelines by the Department of Laboratory Animal Care at the La Jolla Institute for Immunology (LJI) and all surgical procedures were done following the protocol approved by the Animal Care Committee of LJI.

hITGB2 KI mice were generated by GenOway (Lyon, France) by knocking in a gene cassette coding for the cDNA of human *ITGB2* isoform 1 to the mouse *Itgb2* locus. The gene cassette was inserted in frame with the ATG in exon 2. This insertion of the cassette resulted in the disruption of the endogenous gene and no mouse *Itgb2* (mItgb2) was expressed. Homologous recombination was performed in C57BL/6N-derived embryonic stem cell line. To excise the FRT-flanked Neomycin resistance cassette and generate the final heterozygous humanized knock-in animals, chimeras were bred with C57BL/6N FLP-recombinase expressing females. Subsequently, mice were bred to generate homozygous human ITGB2 KI mice. hITGB2 expression and mItgb2 deletion were validated by PCR and flow cytometry using fluorophore-conjugated anti-hCD18 (clone TS1/18) and anti-mCD18 (clone GAME-46).

METHOD DETAILS

Induction of septic shock in mice—Mice were injected i.p. with 40 mg/kg LPS (E. coli, strain O55:B5; Sigma-Aldrich) that was dissolved in sterile PBS at 10 mg/mL concentration (Marki et al., 2021). This treatment induces severe septic shock to which the mice succumb within 24 h (Soromou et al., 2014). 6 h after treatment, mouse whole blood was collected via retro-orbital bleeding or heart cardiac puncture. For preparation of single cells from mouse lung tissues, the mouse lung was rinsed with ice-cold PBS and transferred to a gentleMACS C tube (Miltenyi Biotec) and digested with 2 mg/mL collagenase and 80 U/mL DNase I for 30 min at 37°C on a gentleMACS Dissociator (Miltenyi Biotec). For preparation of single cells from mouse liver tissues, a mechanical disruption protocol was used (Blom et al., 2009). The mouse liver was rinsed with ice-cold PBS, minced with scissors into the first liver suspension (50 mL) and centrifuged at 60 g for 1 min at 22C. The top 45 mL was transferred and centrifuged at 480 g for 8 min at 22°C. The cell pellet was resuspended in 10 mL 37.5% Percoll containing heparin, followed by centrifugation at 850 g for 30 min at 22°C. The pellet was resuspended in RBC lysis buffer (eBioscience) followed by centrifugation for 8 min at 4°C and resuspend in FACS buffer (PBS containing 2%FBS and 1 mM EDTA). The mouse whole blood, lung, and liver cell numbers were counted using a Hemavet 950 (Drew Scientific).

Histology—Lungs and livers were collected, rinsed in PBS, fixed in 20:1 fixative (zinc formalin): tissue volume for 72 h at 4°C, transferred to 70% isopropyl alcohol, cut into three strips, and placed in histology cassettes. Samples were then embedded in paraffin, and cut into 4-μm sections. The tissues were stained with hematoxylin and eosin (H&E) and

periodic acid-Schiff (PAS) for histopathologic assessment by a board-certified pathologist. Slides were digitized on AxioScan Z1 slide scanner using 40 ×0.95NA objective (Zeiss).

Flow cytometry/stimulation assay—Heparinized whole blood was obtained from healthy human donors. Mouse whole blood was collected via retro-orbital bleeding or cardiac heart puncture. Red blood cells were lysed by mixing 1 part of blood and 9 parts of ice-cold water for 15 s and then resuspended in 1xPBS. Bone marrow cells were flushed from both femurs and tibias. Cells were resuspended in 200 μL FACS staining buffer. Cells were stained with BD Horizon™ Fixable Viability Stain 700 (FVS700) for analysis of viability for 15 min at 4°C. Surface antigens on cells were stained for 30 min at 4°C with directly conjugated fluorescent antibodies. Forward-and side-scatter parameters were used for exclusion of doublets from analysis. Cell fluorescence was assessed with a LSRII (BD Biosciences) and was analyzed with FlowJo (BD, version 10.4). Gating scheme was shown in Figure S1.

For real time stimulation assay, cells were resuspended in RPMI-1640 media without phenol red supplemented with 2% human serum albumin. The dynamic antibody binding was recorded with a LSRII flow cytometer (BD Biosciences). mAb24 and KIM127 (1 μg/mL) were incubated with cells for 150 s before adding IL-8 (100 ng/mL) or CXCL1 (10 ng/mL) to the tube.

Intravital imaging—The mouse cremaster muscle was prepared for intravital imaging of the microcirculation as described (Liu et al., 2005; Marki et al., 2018; Wen et al., 2018, 2021). Male hITGB2 KI mice were anesthetized with isoflurane/oxygen inhalation and placed on a 37°C heating pad. The left carotid artery was cannulated with a polyethylene-10 tube (BD) for injection of antibodies and stimuli. The left cremaster muscle was exteriorized, cut open with a thermal cautery and pinned in a flat position to the imaging pedestal of a custom-built imaging platform. Cremaster venules were imaged with a Leica 25×/0.95 NA water-immersion objective on a Leica SP8 confocal microscope (Leica Microsystems) equipped with a resonant scanner. To visualize the neutrophils and β_2 integrin conformations, the mouse was injected with 2.5 μg mAb24-AlexaFluor 488 (AF488), KIM127-Dylight 550 (DL550) and Ly6G-AlexaFluor 647 (AF647) antibodies via the carotid cannula. About three minutes after that, 300 ng of murine CXCL1 was injected in 100 μL PBS through the carotid cannula. A triple dichroic 488/552/638 nm excitation beam splitter was used. To detect the signal of mAb24-AF488 and KIM127-DL550, the tissue was illuminated with 488 nm and 552 nm lasers and the range of the HyD detectors set to 496–542 nm and 557–615 nm, respectively. To detect the signal of Ly6G-AF647, the tissue was illuminated with 638 nm laser and the PMT detector was set to the range of 644–770 nm. Three channels were acquired in a sequential line switch mode with a pinhole set to 2 Airy units, zoom 1.75, line average 16, frame size x:1024-y:256 pixel, and frame time of 500 ms. Glass micropipettes were used to inject 10 μM fMLP locally into cremaster muscle to induce neutrophil transmigration.

Microfluidic perfusion assay—The assembly of the multichannel microfluidic devices used in this study has been described previously (Fan et al., 2016; Sundd et al., 2011; Wen

et al., 2020). Glass coverslips were coated with mouse P-selectin-Fc (2 μg/mL), ICAM-1-Fc (10 μg/mL) for 2 h and then blocked for 1 h with casein (1%) at room temperature. After coating, coverslips were sealed to polydimethylsiloxane chips by magnetic clamps to create flow chamber channels ~29 μm high and ~300 μm across. By modulating the pressure between the inlet well and the outlet reservoir, a 6 dyn/cm^2 wall shear stress was applied in all experiments. For the perfusion of mouse primary neutrophils in the microfluidics, harvested mouse bone marrow cells were labeled with anti-mouse Ly-6G antibody and perfused in the microfluidic device over a substrate of recombinant murine P-selectin-Fc, recombinant murine ICAM-1-Fc. CXCL1 (10 ng/mL) was added in the inlet well to induce mouse neutrophil adhesion.

Triple-color qDF imaging—The qDF setup and the theory of qDF have been described previously in detail (Sundd et al., 2010, 2011; Wen et al., 2020). The setup was based on an IX71 inverted TIRF research microscope (Olympus) equipped with a 100x NA 1.45 plan-apochromatic oil immersion TIRFM objective and 30 mW 488 nm, 20 mW 561 nm and 5 mW 641 nm diode-pumped-solid-state lasers (CVI Melles Griot) as TIRF excitation light sources. A TIRF incidence angle of 70°was used for all three lasers in all qDF experiments. Images were captured at an interval of every 1–2 s using a 16-bit digital CCD camera (Hamamatsu C10600–10B ORCA-R^2). The laser shutters and camera were controlled with the SlideBook5.5 software (Intelligent Imaging Innovations Inc.). Fluorescence channels were separated using a beam splitter (QV^2 QuadView; Photometrics) equipped with two dichroic mirrors (560 nm and 660 nm) and three emission filters (525/50 nm, 600/32 nm, and 700/75 nm).

QUANTIFICATION AND STATISTICAL ANALYSIS

Image analysis—Offline image analysis was done using ImagePro 10 (Media Cybernetics) and Fiji (Schindelin et al., 2012). For further data evaluation, Microsoft Excel (Microsoft), Graphpad Prism 9 were used. Raw qDF images were used to generate binary masks using ‘Smart Segmentation’ in ImagePro (Wen et al., 2021). Integrin clusters were identified by generating the binary mask. ‘Smart Segmentation’ is a pixel classification algorithm which uses reference objects to define classes based on pixel intensities. Subsequently, each pixel in the image was analyzed and compared to the values of the reference objects and assigned to the class of the closest reference object. Different from simple thresholding, ‘Smart Segmentation’ can identify clusters by comparing each cluster with its local background. The number and area of clusters were quantified using the ‘analyze particles’ function in Fiji. For intravital imaging, segmentation was generated based on the Ly-6G labeling which outlines the neutrophils. Then, mean fluorescence intensities (MFI) were calculated using Fiji. For analysis of the distribution of mAb24 and KIM127 distribution, a line (1 pixel wide) was drawn along the cell top, front, bottom, and rear of each neutrophil using the plot profile function in Fiji, and profiles of mAb24 and KIM127 fluorescence intensities were measured as a function of location. To average the signals, mAb24, KIM127 and the product KIM127 x mAb24 were each normalized, so the average intensity was equal to 1. The normalized data were distributed into 40 bins using the *stat_summary_bin* function, and the mean ± range for each bin as well as the significance for being different from 1 were calculated and plotted with the R package ggplot2.

Statistics—Data are expressed as mean ± SEM. Statistical analysis was performed with Graphpad Prism software. For comparisons between 2 groups, 2-tailed Student t tests were performed. Data normality were checked using both Kolmogorov-Smirnov test and Shapiro-Wilk tests. In cases of data not passing normality test, a non-parametric test (Mann–Whitney U test) was applied. Statistical differences between more than two groups were analyzed by one-way ANOVA followed by Tukey's multiple comparison test. For parametric data, statistical significance was analyzed using Student's t-test (or Welch t-test for samples with non-equal variances). Statistics for Figure 4F was performed by a one sample t-test with Benjamini-Hochberg correction, comparing the overall average (mu =1) to each binned data point's average. p values <0.05 were considered significant. The significance level of p values is indicated by asterisks (*p < 0.05; **p < 0.01; ***p < 0.001; ****p < 0.0001; n.s., not significant).

Supplementary Material

Refer to Web version on PubMed Central for supplementary material.

ACKNOWLEDGMENTS

We would like to thank the LJI Flow Cytometry Core for their expert assistance with our research. This work was supported by grants from the National Institutes of Health, USA (HL078784 to K.L.) and a Postdoctoral Fellowship and a Career Development Award (19POST34450228 and 942098 to L.W.) from the American Heart Association, USA.

REFERENCES

Alon R, and Shulman Z. (2011). Chemokine triggered integrin activation and actin remodeling events guiding lymphocyte migration across vascular barriers. Exp. Cell Res 317, 632–641. 10.1016/j.yexcr.2010.12.007. [PubMed: 21376176]

Alves-Filho JC, Spiller F, and Cunha FQ (2010). Neutrophil paralysis in sepsis. Shock 34 (Suppl 1), 15–21. 10.1097/shk.0b013e3181e7e61b. [PubMed: 20714263]

Anderson DC, and Springer TA (1987). Leukocyte adhesion deficiency: an inherited defect in the Mac-1, LFA-1, and p150,95 glycoproteins. Annu. Rev. Med 38, 175–194. 10.1146/annurev.me.38.020187.001135. [PubMed: 3555290]

Bachmann MF, McKall-Faienza K, Schmits R, Bouchard D, Beach J, Speiser DE, Mak TW, and Ohashi PS (1997). Distinct roles for LFA-1 and CD28 during activation of naive T cells: adhesion versus costimulation. Immunity 7, 549–557. 10.1016/s1074-7613(00)80376-3. [PubMed: 9354475]

Blom KG, Rahman Qazi M, Noronha Matos JB, Nelson BD, DePierre JW, and Abedi-Valugerdi M. (2009). Isolation of murine intrahepatic immune cells employing a modified procedure for mechanical disruption and functional characterization of the B, T and natural killer T cells obtained. Clin. Exp. Immunol 155, 320–329. 10.1111/j.1365-2249.2008.03815.x. [PubMed: 19040612]

Bouaouina M, Blouin E, Halbwachs-Mecarelli L, Lesavre P, and Rieu P. (2004). TNF-induced β_2 Integrin activation involves src kinases and a redox-regulated activation of p38 MAPK. J. Immunol 173, 1313–1320. 10.4049/jimmunol.173.2.1313. [PubMed: 15240725]

Chigaev A, Waller A, Amit O, Halip L, Bologa CG, and Sklar LA (2009). Real-time analysis of conformation-sensitive antibody binding provides new insights into integrin conformational regulation. J. Biol. Chem 284, 14337–14346. 10.1074/jbc.m901178200. [PubMed: 19251697]

Damiano ER, Westheider J, Tozeren A, and Ley K. (1996). Variation in the velocity, deformation, and adhesion energy density of leukocytes rolling within venules. Circ. Res 79, 1122–1130. 10.1161/01.res.79.6.1122. [PubMed: 8943950]

Danikas DD, Karakantza M, Theodorou GL, Sakellaropoulos GC, and Gogos CA (2008). Prognostic value of phagocytic activity of neutrophils and monocytes in sepsis. Correlation to CD64 and CD14

antigen expression. Clin. Exp. Immunol 154, 87–97. 10.1111/j.1365-2249.2008.03737.x. [PubMed: 18727624]

Dembo M, Torney DC, Saxman K, and Hammer D. (1988). The reaction-limited kinetics of membrane-to-surface adhesion and detachment. Proc. R. Soc. Lond. B Biol. Sci 234, 55–83. 10.1098/rspb.1988.0038. [PubMed: 2901109]

Downey GP, Doherty DE, Schwab B 3rd, Elson EL, Henson PM, and Worthen GS (1990). Retention of leukocytes in capillaries: role of cell size and deformability. J. Appl. Physiol 69, 1767–1778. 10.1152/jappl.1990.69.5.1767. [PubMed: 2272970]

Dransfield I, and Hogg N. (1989). Regulated expression of Mg2+ binding epitope on leukocyte integrin alpha subunits. EMBO J. 8, 3759–3765. 10.1002/j.1460-2075.1989.tb08552.x. [PubMed: 2479549]

Fagerholm SC, Guenther C, Llort Asens M, Savinko T, and Uotila LM (2019). Beta2-Integrins and interacting proteins in leukocyte trafficking, immune suppression, and immunodeficiency disease. Front Immunol. 10, 254. 10.3389/fimmu.2019.00254. [PubMed: 30837997]

Fan Z, Kiosses WB, Sun H, Orecchioni M, Ghosheh Y, Zajonc DM, Arnaout MA, Gutierrez E, Groisman A, Ginsberg MH, and Ley K. (2019). High-affinity bent β_2-integrin molecules in arresting neutrophils face each other through binding to ICAMs in cis. Cell Rep 26, 119–130.e5. 10.1016/j.celrep.2018.12.038. [PubMed: 30605669]

Fan Z, McArdle S, Marki A, Mikulski Z, Gutierrez E, Engelhardt B, Deutsch U, Ginsberg M, Groisman A, and Ley K. (2016). Neutrophil recruitment limited by high-affinity bent β_2 integrin binding ligand in cis. Nat. Commun 7, 12658. 10.1038/ncomms12658. [PubMed: 27578049]

Galkina E, Thatte J, Dabak V, Williams MB, Ley K, and Braciale TJ (2005). Preferential migration of effector CD8+ T cells into the interstitium of the normal lung. J. Clin. Invest 115, 3473–3483. 10.1172/jci24482. [PubMed: 16308575]

Gupta V, Gylling A, Alonso JL, Sugimori T, Ianakiev P, Xiong JP, and Amin Arnaout M. (2007). The β-tail domain (βTD) regulates physiologic ligand binding to integrin CD11b/CD18. Blood 109, 3513–3520. 10.1182/blood-2005-11-056689. [PubMed: 17170130]

Hynes RO (2002). Integrins: bidirectional, allosteric signaling machines. Cell 110, 673–687. 10.1016/s0092-8674(02)00971-6. [PubMed: 12297042]

Hyun YM, Sumagin R, Sarangi PP, Lomakina E, Overstreet MG, Baker CM, Fowell DJ, Waugh RE, Sarelius IH, and Kim M. (2012). Uropod elongation is a common final step in leukocyte extravasation through inflamed vessels. J. Exp. Med 209, 1349–1362. 10.1084/jem.20111426. [PubMed: 22711877]

Jankowska KI, Williamson EK, Roy NH, Blumenthal D, Chandra V, Baumgart T, and Burkhardt JK (2018). Integrins modulate T cell receptor signaling by constraining actin flow at the immunological synapse. Front Immunol. 9, 25. 10.3389/fimmu.2018.00025. [PubMed: 29403502]

Kolaczkowska E, and Kubes P. (2013). Neutrophil recruitment and function in health and inflammation. Nat. Rev. Immunol 13, 159–175. 10.1038/nri3399. [PubMed: 23435331]

Koltsova EK, Garcia Z, Chodaczek G, Landau M, McArdle S, Scott SR, von Vietinghoff S, Galkina E, Miller YI, Acton ST, and Ley K. (2012). Dynamic T cell-APC interactions sustain chronic inflammation in atherosclerosis. J. Clin. Invest 122, 3114–3126. 10.1172/jci61758. [PubMed: 22886300]

Krauss JC, Bond LM, Todd RF 3rd, and Wilson JM (1991). Expression of retroviral transduced human CD18 in murine cells: an in vitro model of gene therapy for leukocyte adhesion deficiency. Hum. Gene Ther 2, 221–228. 10.1089/hum.1991.2.3-221. [PubMed: 1684295]

Kunkel EJ, Dunne JL, and Ley K. (2000). Leukocyte arrest during cytokinedependent inflammation in vivo. J. Immunol 164, 3301–3308. 10.4049/jimmunol.164.6.3301. [PubMed: 10706723]

Kuwano Y, Spelten O, Zhang H, Ley K, and Zarbock A. (2010). Rolling on E- or P-selectin induces the extended but not high-affinity conformation of LFA-1 in neutrophils. Blood 116, 617–624. 10.1182/blood-2010-01-266122. [PubMed: 20445017]

Lefort CT, Rossaint J, Moser M, Petrich BG, Zarbock A, Monkley SJ, Critchley DR, Ginsberg MH, Fassler R, and Ley K. (2012). Distinct roles for talin-1 and kindlin-3 in LFA-1 extension and affinity regulation. Blood 119, 4275–4282. 10.1182/blood-2011-08-373118. [PubMed: 22431571]

Ley K, Hoffman HM, Kubes P, Cassatella MA, Zychlinsky A, Hedrick CC, and Catz SD (2018). Neutrophils: new insights and open questions.Sci. Immunol 3. 10.1126/sciimmunol.aat4579.

Ley K, Laudanna C, Cybulsky MI, and Nourshargh S. (2007). Getting to the site of inflammation: the leukocyte adhesion cascade updated. Nat. Rev. Immunol 7, 678–689. 10.1038/nri2156. [PubMed: 17717539]

Ley K, Rivera-Nieves J, Sandborn WJ, and Shattil S. (2016). Integrin-based therapeutics: biological basis, clinical use and new drugs. Nat. Rev. Drug Discov 15, 173–183. 10.1038/nrd.2015.10. [PubMed: 26822833]

Liu L, Cara DC, Kaur J, Raharjo E, Mullaly SC, Jongstra-Bilen J, Jongstra J, and Kubes P. (2005). LSP1 is an endothelial gatekeeper of leukocyte transendothelial migration. J. Exp. Med 201, 409–418. 10.1084/jem.20040830. [PubMed: 15684321]

Maiguel D, Faridi MH, Wei C, Kuwano Y, Balla KM, Hernandez D, Barth CJ, Lugo G, Donnelly M, Nayer A, et al. (2011). Small molecule-mediated activation of the integrin CD11b/CD18 reduces inflammatory disease. Sci. Signal 4, ra57. 10.1126/scisignal.2001811.

Marki A, Buscher K, Lorenzini C, Meyer M, Saigusa R, Fan Z, Yeh YT, Hartmann N, Dan JM, Kiosses WB, et al. (2021). Elongated neutrophil-derived structures are blood-borne microparticles formed by rolling neutrophils during sepsis. J. Exp. Med 218. 10.1084/jem.20200551.

Marki A, Buscher K, Mikulski Z, Pries A, and Ley K. (2018). Rolling neutrophils form tethers and slings under physiologic conditions in vivo. J. Leukoc. Biol 103, 67–70. 10.1189/jlb.1AB0617-230R. [PubMed: 28821572]

Marki A, Gutierrez E, Mikulski Z, Groisman A, and Ley K. (2016). Microfluidics-based side view flow chamber reveals tether-to-sling transition in rolling neutrophils. Scientific Rep. 6, 28870. 10.1038/srep28870.

McArdle S, Buscher K, Ghosheh Y, Pramod AB, Miller J, Winkels H, Wolf D, and Ley K. (2019). Migratory and dancing macrophage subsets in atherosclerotic lesions. Circ. Res 125, 1038–1051. 10.1161/circresaha.119.315175. [PubMed: 31594470]

Morikis VA, Chase S, Wun T, Chaikof EL, Magnani JL, and Simon SI (2017). Selectin catch-bonds mechanotransduce integrin activation and neutrophil arrest on inflamed endothelium under shear flow. Blood 130, 2101–2110. 10.1182/blood-2017-05-783027. [PubMed: 28811304]

Muller Kobold AC, Tulleken JE, Zijlstra JG, Sluiter W, Hermans J, Kallenberg CGM, and Cohen Tervaert JW (2000). Leukocyte activation in sepsis; correlations with disease state and mortality. Intensive Care Med. 26, 883–892. 10.1007/s001340051277. [PubMed: 10990102]

Nourshargh S, and Alon R. (2014). Leukocyte migration into inflamed tissues. Immunity 41, 694–707. 10.1016/j.immuni.2014.10.008. [PubMed: 25517612]

Pittet MJ, and Weissleder R. (2011). Intravital imaging. Cell 147, 983–991. 10.1016/j.cell.2011.11.004. [PubMed: 22118457]

Pospieszalska MK, Lasiecka I, and Ley K. (2011). Cell protrusions and tethers: a unified approach. Biophys. J 100, 1697–1707. 10.1016/j.bpj.2011.02.038. [PubMed: 21463583]

Robinson MK, Andrew D, Rosen H, Brown D, Ortlepp S, Stephens P, and Butcher EC (1992). Antibody against the Leu-CAM beta-chain (CD18) promotes both LFA-1- and CR3-dependent adhesion events. J. Immunol148, 1080–1085. [PubMed: 1371129]

Scharffetter-Kochanek K, Lu H, Norman K, van Nood N, Munoz F, Grabbe S, McArthur M, Lorenzo I, Kaplan S, Ley K, et al. (1998). Spontaneous skin ulceration and defective T cell function in CD18 null mice. J. Exp.Med 188, 119–131. 10.1084/jem.188.1.119. [PubMed: 9653089]

Schindelin J, Arganda-Carreras I, Frise E, Kaynig V, Longair M, Pietzsch T, Preibisch S, Rueden C, Saalfeld S, Schmid B, et al. (2012). Fiji: an open-source platform for biological-image analysis. Nat. Methods 9, 676–682. 10.1038/nmeth.2019. [PubMed: 22743772]

Schneider CA, Rasband WS, and Eliceiri KW (2012). NIH Image to ImageJ: 25 years of image analysis. Nature Methods 9, 671–675. [PubMed: 22930834]

Shattil SJ, Kim C, and Ginsberg MH (2010). The final steps of integrin activation: the end game. Nat. Rev. Mol. Cell Biol 11, 288–300. 10.1038/nrm2871. [PubMed: 20308986]

Shimaoka M, Xiao T, Liu JH, Yang Y, Dong Y, Jun CD, McCormack A, Zhang R, Joachimiak A, Takagi J, et al. (2003). Structures of the alpha L I domain and its complex with

ICAM-1 reveal a shape-shifting pathway for integrin regulation. Cell 112, 99–111. 10.1016/s0092-8674(02)01257-6. [PubMed: 12526797]

Simon SI, Sarantos MR, Green CE, and Schaff UY (2009). Leucocyte recruitment under fluid shear: mechanical and molecular regulation within the inflammatory synapse. Clin. Exp. Pharmacol. Physiol 36, 217–224. 10.1111/j.1440-1681.2008.05083.x. [PubMed: 19018799]

Smith DF, Deem TL, Bruce AC, Reutershan J, Wu D, and Ley K. (2006). Leukocyte phosphoinositide-3 kinase γ is required for chemokineinduced, sustained adhesion under flow in vivo. J. Leukoc. Biol 80, 1491–1499. 10.1189/jlb.0306227. [PubMed: 16997858]

Sonego F, Castanheira FV, Ferreira RG, Kanashiro A, Leite CA, Nascimento DC, Colon DF, Borges Vde F, Alves-Filho JC, and Cunha FQ (2016). Paradoxical Roles of the Neutrophil in Sepsis: Protective and Deleterious. Front Immunol 7, 155. 10.3389/fimmu.2016.00155. [PubMed: 27199981]

Soromou LW, Jiang L, Wei M, Chen N, Huo M, Chu X, Zhong W, Wu Q, Balde A, Deng X, and Feng H. (2014). Protection of mice against lipopolysaccharide-induced endotoxic shock by pinocembrin is correlated with regulation of cytokine secretion. J. Immunotoxicol 11, 56–61. 10.3109/1547691x.2013.792886. [PubMed: 23697399]

Springer TA, and Dustin ML (2012). Integrin inside-out signaling and the immunological synapse. Curr. Opin. Cel. Biol 24, 107–115. 10.1016/j.ceb.2011.10.004.

Sundd P, Gutierrez E, Petrich BG, Ginsberg MH, Groisman A, and Ley K. (2011). Live cell imaging of paxillin in rolling neutrophils by dual-color quantitative dynamic footprinting. Microcirculation 18, 361–372. 10.1111/j.1549-8719.2011.00090.x. [PubMed: 21418380]

Sundd P, Gutierrez E, Pospieszalska MK, Zhang H, Groisman A, and Ley K. (2010). Quantitative dynamic footprinting microscopy reveals mechanisms of neutrophil rolling. Nat. Methods 7, 821–824. 10.1038/nmeth.1508. [PubMed: 20871617]

Tozeren A, and Ley K. (1992). How do selectins mediate leukocyte rolling in venules? Biophys. J 63, 700–709. 10.1016/s0006-3495(92)81660-0. [PubMed: 1420908]

van de Vijver E, Maddalena A, Sanal O, Holland SM, Uzel G, Madkaikar M, de Boer M, van Leeuwen K, Koker MY, Parvaneh N, et al. (2012). Hematologically important mutations: leukocyte adhesion deficiency (first update). Blood Cells Mol. Dis 48, 53–61. 10.1016/j.bcmd.2011.10.004. [PubMed: 22134107]

Wen L, Fan Z, Mikulski Z, and Ley K. (2020). Imaging of the immune system - towards a subcellular and molecular understanding. J. Cell Sci 133. 10.1242/jcs.234922.

Wen L, Feil S, Wolters M, Thunemann M, Regler F, Schmidt K, Friebe A, Olbrich M, Langer H, Gawaz M, et al. (2018). A shear-dependent NOcGMP-cGKI cascade in platelets acts as an auto-regulatory brake of thrombosis. Nat. Commun 9, 4301. 10.1038/s41467-018-06638-8. [PubMed: 30327468]

Wen L, Marki A, Roy P, McArdle S, Sun H, Fan Z, Gingras AR, Ginsberg MH, and Ley K. (2021). Kindlin-3 recruitment to the plasma membrane precedes high-affinity β_2-integrin and neutrophil arrest from rolling. Blood 137, 29–38. 10.1182/blood.2019003446. [PubMed: 32777822]

Wen L, Moser M, and Ley K. (2022). Molecular mechanisms of leukocyte Beta2 integrin activation. Blood.

Wolf D, Anto-Michel N, Blankenbach H, Wiedemann A, Buscher K, Hohmann JD, Lim B, Bauml M, Marki A, Mauler M, et al. (2018). A ligand-specific blockade of the integrin Mac-1 selectively targets pathologic inflammation while maintaining protective host-defense. Nat. Commun 9, 525. 10.1038/s41467-018-02896-8. [PubMed: 29410422]

Yago T, Zhang N, Zhao L, Abrams CS, and McEver RP (2018). Selectins and chemokines use shared and distinct signals to activate β_2 integrins in neutrophils. Blood Adv. 2, 731–744. 10.1182/bloodadvances.2017015602. [PubMed: 29592875]

Zarbock A, Lowell CA, and Ley K. (2007). Spleen tyrosine kinase syk is necessary for E-selectin-induced $\alpha L\beta_2$ integrin-mediated rolling on intercellular adhesion molecule-1. Immunity 26, 773–783. 10.1016/j.immuni.2007.04.011. [PubMed: 17543554]

Highlights

- Humanized β_2 integrin knockin mice show β_2 integrin activation *in vivo*
- Activated β_2 integrins accumulate at the rear of neutrophils against blood flow
- Activated β_2 integrins are concentrated at the uropod of neutrophils during TEM
- β_2 integrins are activated in intravascular neutrophils of LPS-treated mice

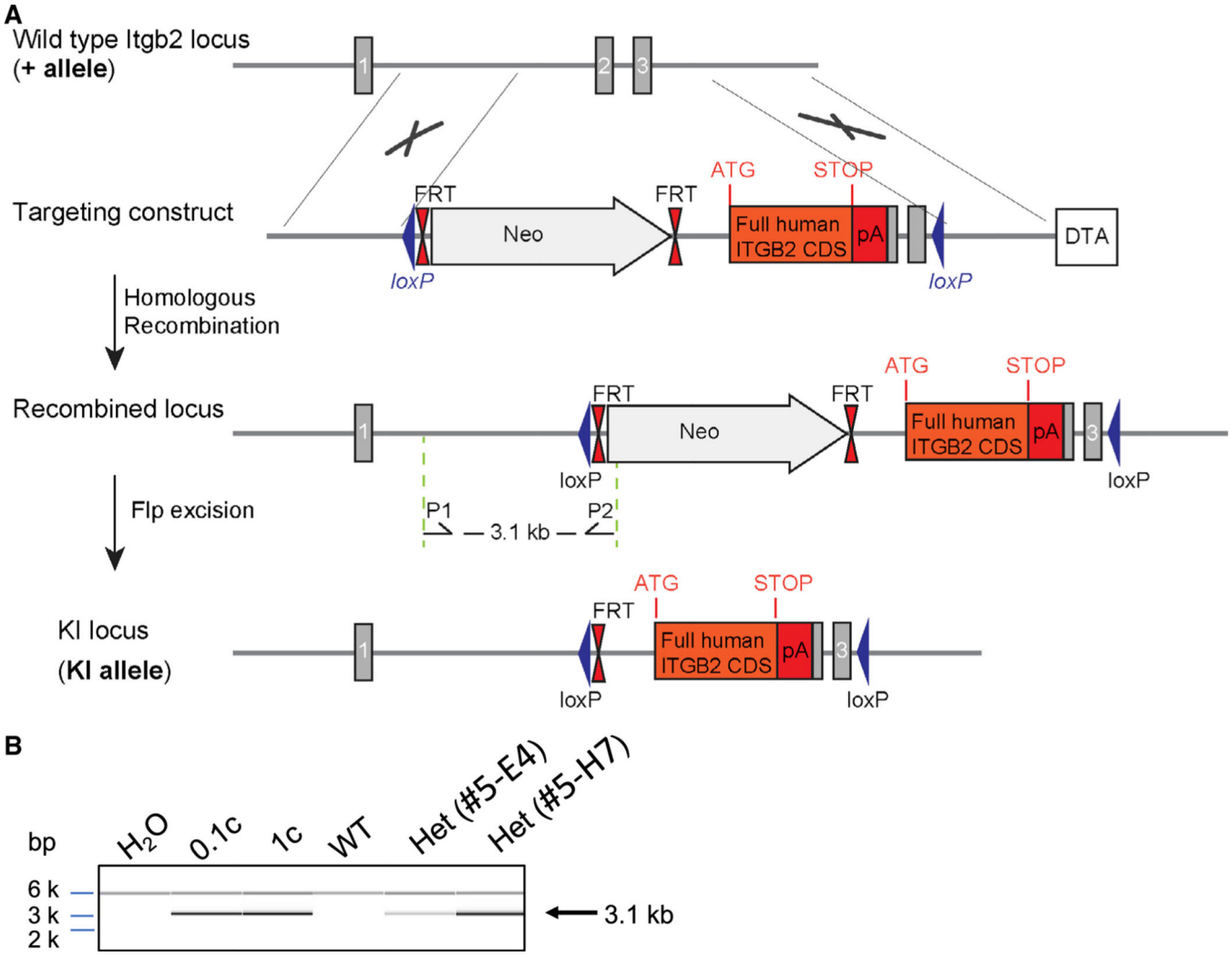

Figure 1. Generation of humanized β_2 integrin knockin mice

(A) Schematic representation of the targeting strategy. Upper panel: wild-type *Itgb2* locus (+ allele). Lower panel: recombined *Itgb2* allele (KI allele). Sequence elements are not depicted to scale. Gray rectangles correspond to *Itgb2* coding exons and solid lines to non-coding sequences. Arrows P1 and P2 correspond to the screening primer binding sites. Gray arrow, neomycin positive-selection cassette; white box, diphtheria toxin A (DTA); blue triangles, LoxP sites; double red triangles, FRT sites; orange box, human *ITGB2* coding sequence; red box, exogenous polyA. The location of the initiation (ATG) and stop (STOP) codons is indicated.

(B) PCR assessment of the recombination event in embryonic stem cell clones over the short homology arm. Correct 5′ recombination is confirmed in the presence of a 3.1 kb PCR product amplified by primers P1 and P2. 0.1c and 1 copies of a positive control vector in the presence of 30 ng of wild-type C57BL/6 genomic DNA (WT) served as positive control. PCR with wild-type DNA (WT) or without DNA (H_2O) served as negative controls. PCR fragments were separated by capillary electrophoresis using AATI ZAG™ Fragment Analyzer and were analyzed using PROSize 2.0 analytical software.

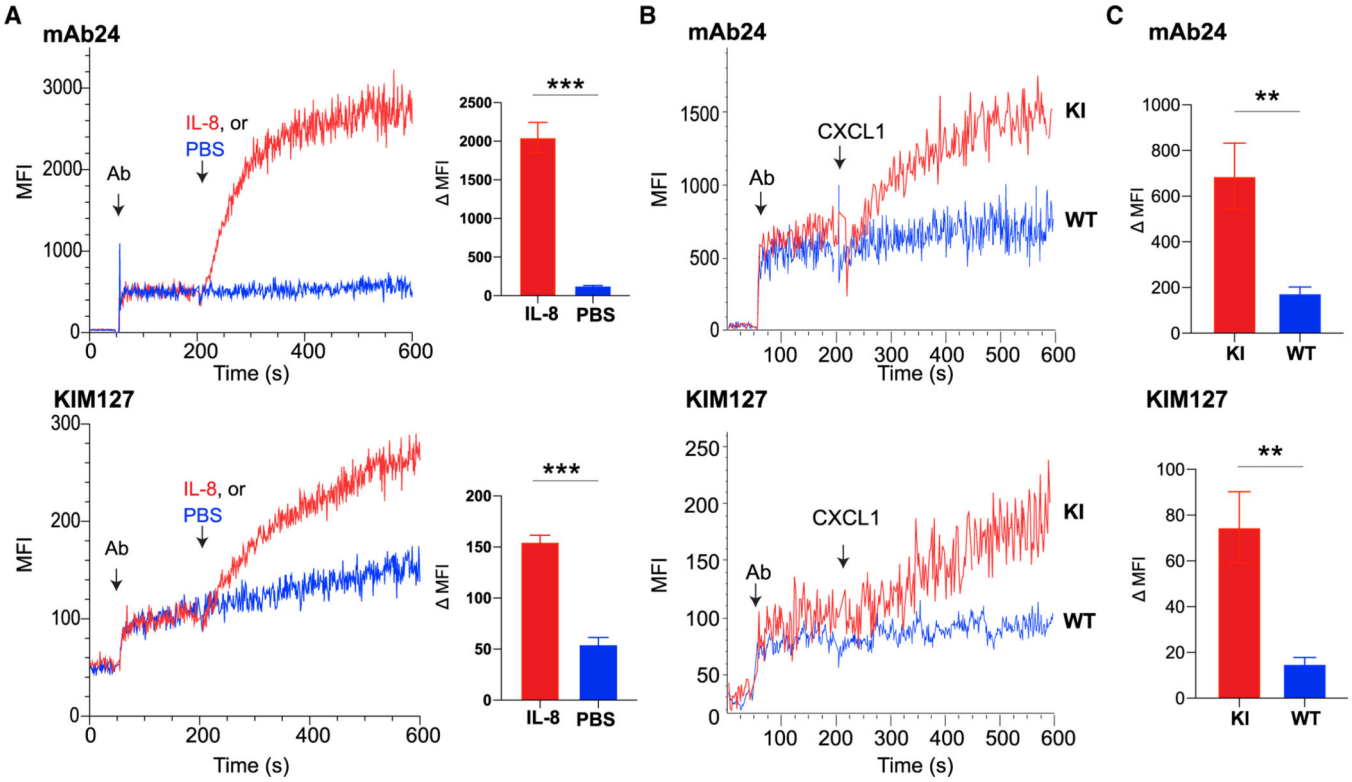

Figure 2. Humanized integrin β_2 mice enable detection of β_2 integrin activation in mouse neutrophils

(A) Human whole blood was incubated with 100 ng/mL IL-8 (added at 200 s) in the presence of the fluorescently labeled, conformation-specific reporters mAb24 and KIM127. Real-time flow cytometry (left) was used to measure the binding of mAb24 and KIM127. Granulocytes were gated by CD66b. The changes in median fluorescence intensity (MFI) after normalization are shown as the difference between intensities at 200 and 600 s (right). Mean ± SEM of three individual experiments in IL-8 and PBS treatment, respectively.

(B) Detection of β_2 integrin activation in hITGB2 KI mouse neutrophils. hITGB2 KI mouse whole blood gated for neutrophils was stimulated by 10 ng/mL CXCL-1 (added at 200 s) in the presence of the fluorescently labeled, conformation-specific reporters mAb24 and KIM127. Gated for live $Ly6G^+$ neutrophils.

(C) Comparison of increases in MFI between 200 and 600 s in homozygous hITGB2 KI and WT mice, respectively. Mean ± SEM of three individual experiments.

**p < 0.01 and ***p < 0.001.

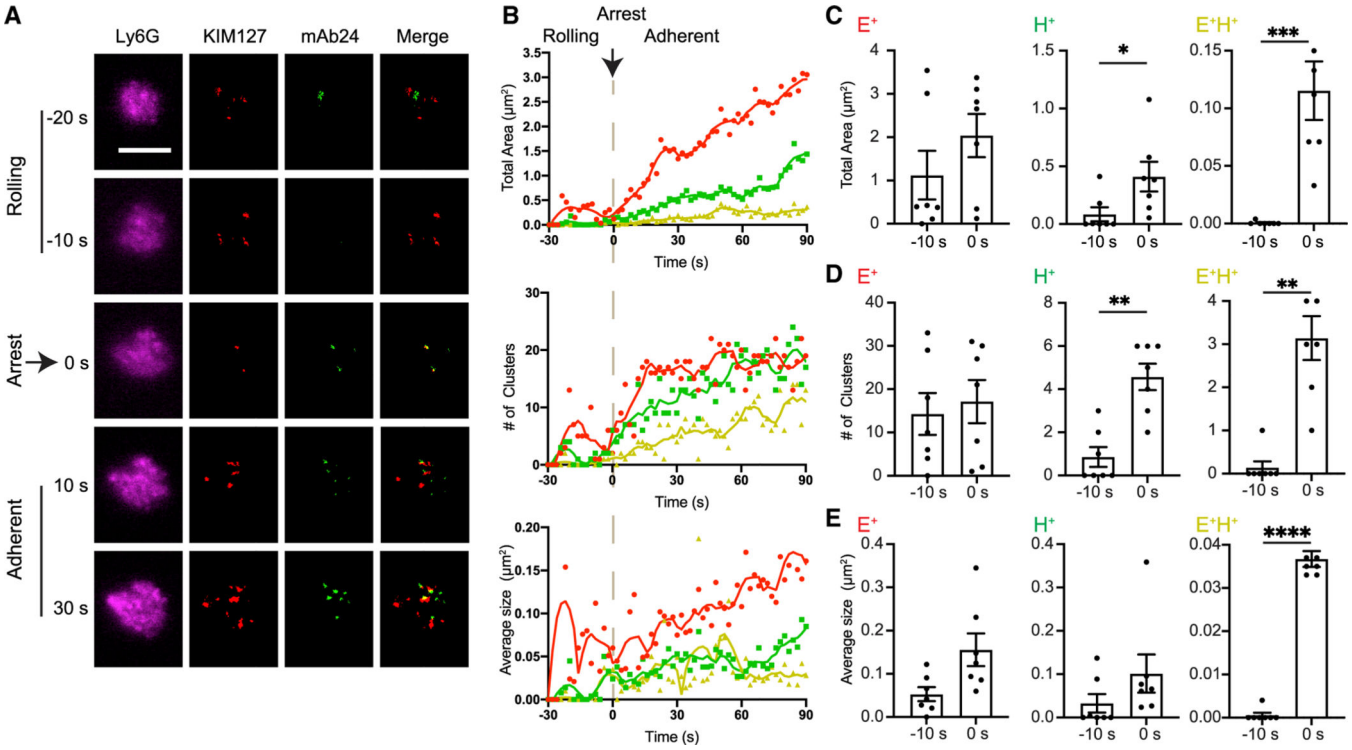

Figure 3. Expression of mAb24 and KIM127 binding epitopes (β_2 integrin E^+ and H^+ conformations) in arresting mouse neutrophils

(A) qDF imaging of the first 150 nm above the coverslip of mouse neutrophils rolling on P-selectin/ICAM-1 substrate. CXCL-1 (10 ng/mL) was perfused at about −20 s in the presence of 1 μg/mL mAb24-Alexa Fluor 488 (mAb24-AF488) and 1 μg/mL KIM127-Dylight 550 (KIM127-DL550). Merge shows mAb24 (green) and KIM127 (red). Scale bar, 5 μm.

(B) Total cluster area, number of clusters, and average cluster area of mAb24-AF488 and KIM127-DL550 antibody-labeled clusters (red, E^+; green, H^+; yellow, E^+H^+) are depicted as a function of time before and after arrest at 0 s.

(C–E) Total cluster area (C), number of clusters (D), and average cluster area (E) of mAb24-AF488 and KIM127-DL550 antibody-labeled clusters (red, E^+; green, H^+; yellow, E^+H^+) before (−10 s) and at the time of arrest at 0 s. Mean ± SEM of 7 cells from three independent experiments are shown.

**p < 0.01; ***p < 0.001; and ****p < 0.0001.

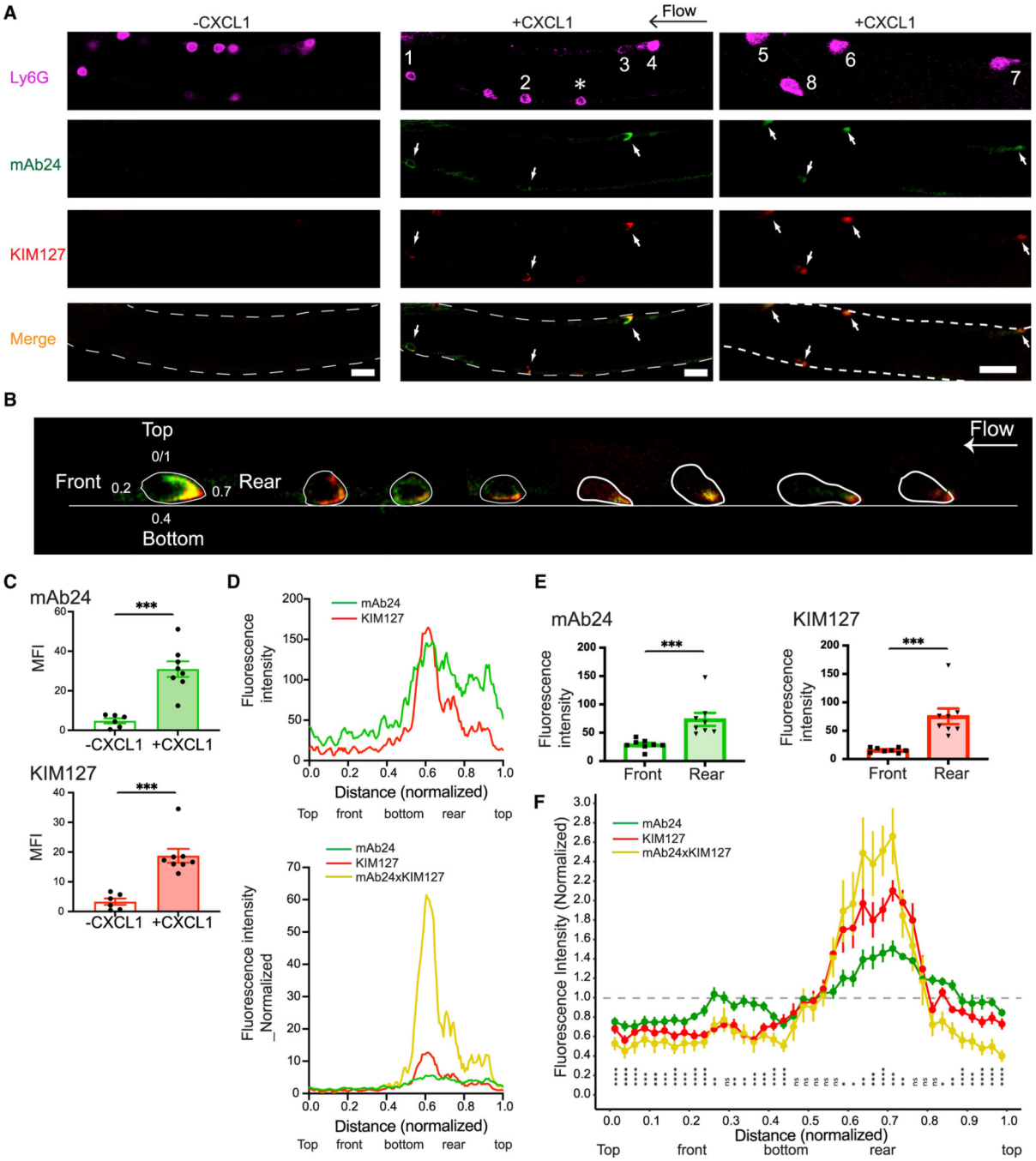

Figure 4. Local β_2 integrin activation in mouse neutrophils arresting in response to CXCL1 *in vivo*

(A) Induction of β_2 extension (KIM127-DL550, red) and high-affinity (mAb24-AF488, green) conformations in mouse neutrophils *in vivo*. Fluorescence images of adherent neutrophils in mouse cremaster muscle venules of hITGB2 KI mice before (left panel) and after (right panel) injection of 300 ng CXCL1 via a carotid artery catheter. White arrows indicate arrested neutrophils. Neutrophils are identified by expression of Ly6G-AF647

(magenta). Horizontal black arrow indicates the direction of blood flow (from right to left). The asterisk indicates a rolling neutrophil. Scale bars, 20 μm.

(B) Eight arrested neutrophils *in vivo* (two mice), showing distribution of activated β_2 integrins.

(C) MFI of mAb24 binding and KIM127 binding before (n = 6 neutrophils) and after (n = 8 neutrophils) CXCL1 treatment.

(D) Upper panel: a line (1 pixel wide using the plot profile function in ImageJ software) was drawn along the cell top, front, bottom, and rear of each neutrophil based on Ly6G labeling. Profiles of mAb24 and KIM127 fluorescence intensities were measured as a function of location. Distance normalized to the circumference of each cell (0–1). Lower panel: profile of mAb24 and KIM127 fluorescence intensities were normalized to average signal intensities. Colocalized signal is represented by the mAb24 signal multiplied by KIM127 signals (mAb24xKIM127, yellow traces).

(E) Statistical comparison of mAb24 and KIM127 fluorescence intensities in the front and rear of neutrophils. Means ± SEM of 8 neutrophils are shown.

(F) Distance around each circumference was normalized (0–1). Intensities for mAb24, KIM127, and the product KIM127 × mAb24 were normalized so that the average intensity was equal to 1 (horizontal line). Data were obtained from 8 neutrophils at 1–2 min after arrest. The normalized data points were binned into 40 intervals and plotted with the R package ggplot2. Point range bars show the range of each binned data point. Statistical analysis was performed for mAb24 × KIM127 by a one-sample t test with Benjamini-Hochberg correction, comparing the overall average ($\mu = 1$) to each binned data point's average.

*$p < 0.05$, **$p < 0.01$, ***$p < 0.001$; ns, not significant.

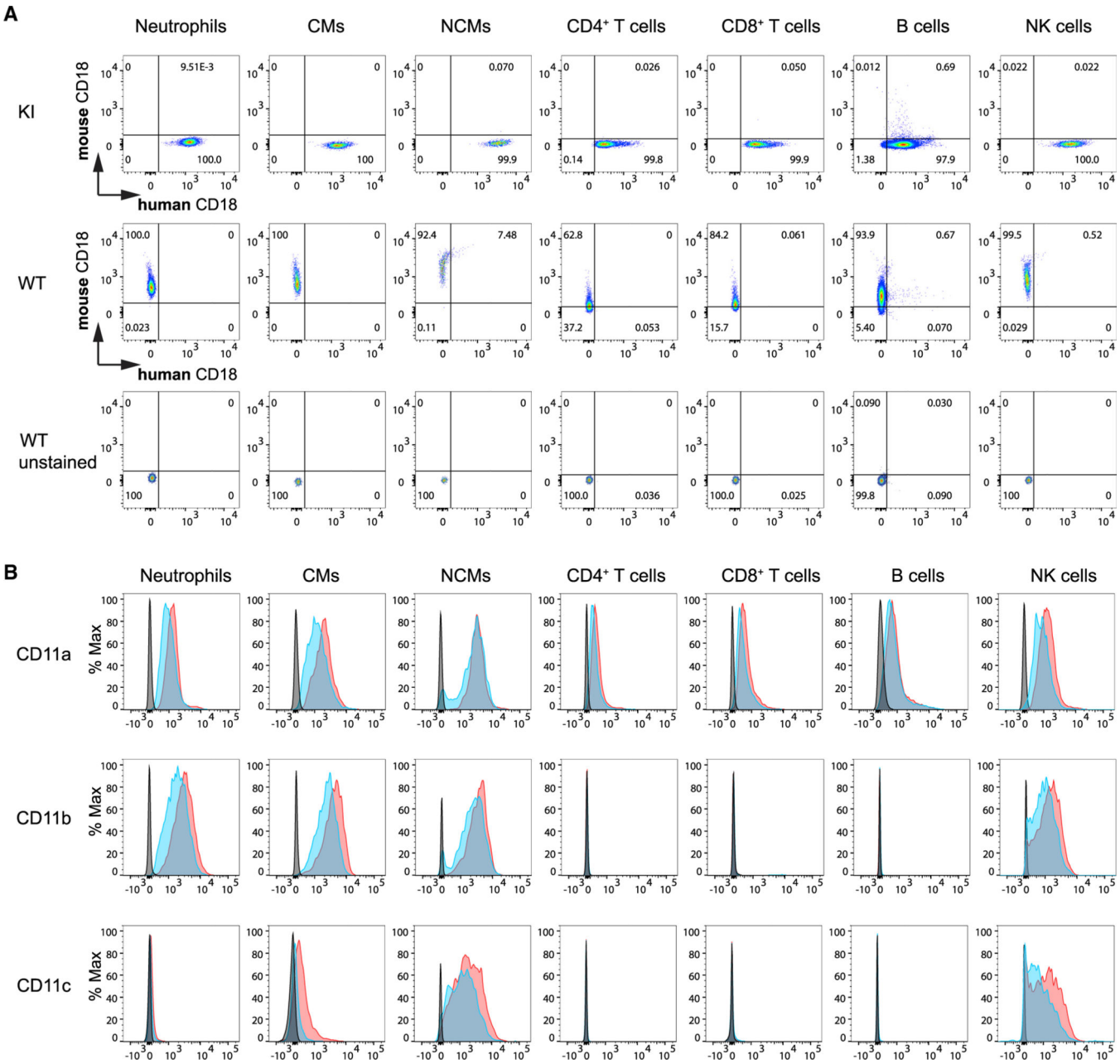

Figure 5. Expression of human integrin β_2 (CD18) in the major mouse leukocyte populations in hITGB2 KI and WT mice

(A) Flow-cytometric analysis of mouse and human CD18 expression in homozygous hITGB2 KI and WT mice, respectively. Mouse whole blood was drawn and red blood cells lysed before staining with anti-human (TS1/18) and mouse (GAME-46) CD18.

(B) Expression of CD11a, CD11b, and CD11c in immune cells of hITGB2 KI mice. After lysis of red blood cells, whole blood of WT (+/+, blue), and homozygous (KI/KI, red) hITGB2 mouse was stained with mAbs to CD11a (upper), CD11b (middle), and CD11c (lower). Gray, unstained control. Representative results of two independent experiments.

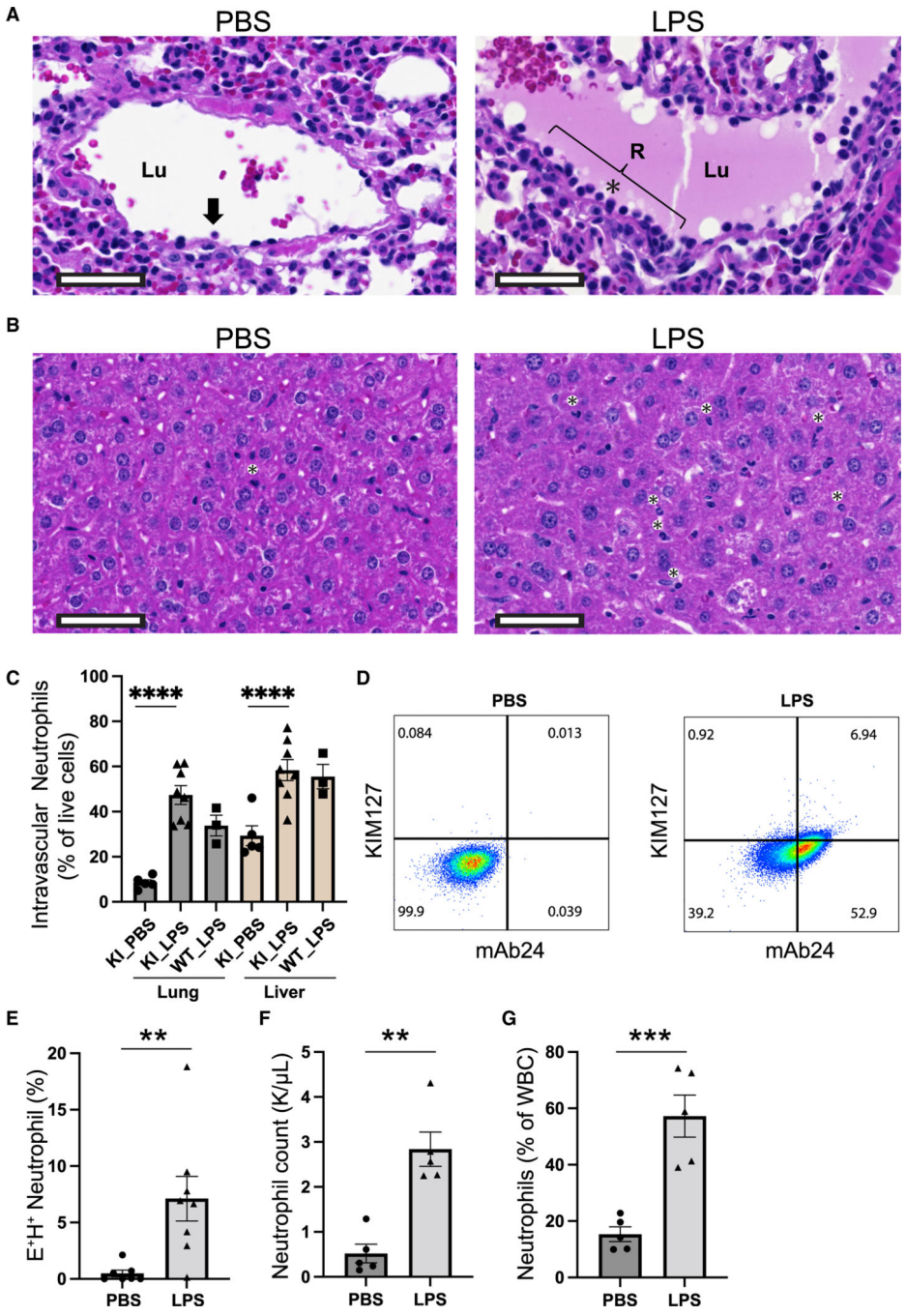

Figure 6. LPS-induced β_2 integrin activation in sepsis

(A and B) Representative H&E photomicrographs of lung (A) and liver (B) tissues from hITGB2 KI mice 6 h after treatment with PBS or LPS. Both lungs and livers were evaluated by a board-certified pathologist. The black arrow or asterisk indicates neutrophils. Lu, lumen; R, area of nucleated cells. Scale bar, 50 μm.

(C) Intravascular neutrophils in total isolated live cells in lung and liver of hITGB2 KI or control WT mice analyzed by FACS. Anti-CD45 was injected intravenously to stain intravascular neutrophils.

(D) Flow-cytometric analysis of integrin activation in whole blood of hITGB2 KI mice after treatment with PBS or LPS.

(E) $mAb24^{+}KIM127^{+}$ ($E^{+}H^{+}$) neutrophils were quantified as mean ± SEM of 7 and 8 mice in PBS and LPS treatment, respectively.

(F and G) Neutrophil count (F) and percentage of neutrophils among total white blood cells (WBCs, G) were measured by Hemavet. Mean ± SEM of 5 mice in PBS and LPS treatment, respectively.

In (C), we performed a one-way ANOVA followed by Tukey's multiple comparison test; in (E)–(G), we performed unpaired Student's t tests. In all tests, **$p < 0.01$; ***$p < 0.001$; and ****$p < 0.0001$.

KEY RESOURCES TABLE

REAGENT or RESOURCE	SOURCE	IDENTIFIER
Antibodies		
Anti-human β_2 integrin (clone mAb24)	Biolegend	Cat# 363402; RRID:AB_2564213
Anti-human β_2 integrin (clone KIM127)	Lymphocyte Culture Center at the University of Virginia	Customized
Anti-human CD66b (clone G10F5)	Biolegend	Cat# 305109; RRID:AB_2563170
Anti-mouse CD18 (clone GAME-46)	BD Biosciences	Cat# 557440; RRID:AB_396703
Anti-mouse CD8a antibody (BUV395, clone 53-6.7)	BD Biosciences	Cat# 563786; RRID:AB_2732919
Anti-mouse Ly-6G (clone 1A8)	Biolegend	Cat# 127610; RRID:AB_1134159
Anti-human CD18 (clone TS1/8)	Biolegend	Cat# 302105; RRID:AB_314223
Anti-mouse Ly-6C (clone HK1.4)	Biolegend	Cat# 128030; RRID:AB_2562617
Anti-mouse CD4 (clone GK1.5)	Biolegend	Cat# 100406; RRID:AB_312691
Anti-mouse CD8a (clone 53-6.7)	Biolegend	Cat# 100721; RRID:AB_312760
Anti-mouse CD19 (clone 6D5)	Biolegend	Cat# 115530; RRID:AB_830707
Anti-mouse TCRb (clone H57-597)	Biolegend	Cat# 109243; RRID:AB_2629564
Anti-mouse CD11a (clone I21/7)	Biolegend	Cat# 153103; RRID:AB_2716033
Anti-mouse CD11b (clone M1/70)	Biolegend	Cat# 101207; RRID:AB_312790
Anti-mouse CD11c (clone N418)	Biolegend	Cat# 117307; RRID:AB_313776
Anti-mouse NK1.1 (clone PK136)	Biolegend	Cat# 108727; RRID:AB_2132706
Anti-mouse CD115 (clone AFS98)	Biolegend	Cat# 135509; RRID:AB_2085222
Anti-mouse CD45.2 Antibody (clone 104)	Biolegend	Cat# 109832; RRID:AB_2565511
Biological samples		
Human blood from healthy donors	LJI	N/A
Chemicals, peptides, and recombinant proteins		
Recombinant human P-selectin-Fc	R&D Systems	Cat# 137-PS-050
Recombinant human ICAM-1-Fc	R&D Systems	Cat# 720-IC-050
Recombinant human IL-8	R&D Systems	Cat# 208-IL-010
Recombinant mouse P-selectin-Fc	R&D Systems	Cat# 737-PS-050
Recombinant mouse ICAM-1-Fc	R&D Systems	Cat# 796-IC-050
Recombinant Mouse CXCL1/KC Protein	R&D Systems	Cat#453-KC-010
Casein blocking buffer	Thermo Fisher	Cat# 37528
Human Serum Albumin	Gemini Bio Products	Cat# 800-120
Lipopolysaccharides from Escherichia coli O55:B5	Sigma-Aldrich	Cat# L2880
N-Formyl-Met-Leu-Phe (fMLP)	Sigma-Aldrich	Cat# F3506-10MG
Critical commercial assays		
DyLight 550 Microscale Antibody Labeling Kit	Thermo Fisher	Cat# 84531
Experimental models: Organisms/strains		

REAGENT or RESOURCE	SOURCE	IDENTIFIER
hITGB2 KI mouse	This paper	Customized
Human: Primary neutrophils	This paper	N/A
Hybridoma of KIM127	ATCC	Cat# CRL-2838 RRID:CVCL_0F09
Oligonucleotides		
Primer for genotyping of hITGB2 KI mice, Forward: GCCTGCCACAGTTTCTCATGTCATAGG	This paper	N/A
Primer for genotyping of hITGB2 KI mice, Reverse: CACCTGATGCCCTGTTTCCGTAGC	This paper	N/A
Software and algorithms		
ImageJ	Schneider et al., 2012	https://imagej.nih.gov/ij/
Prism 9	GraphPad	graphpad.com
Imaris 9.6.0	Oxford Instruments	https://imaris.oxinst.com/
Other		
Roswell Park Memorial Institute (RPMI) medium 1640 without phenol red	Thermo Fisher	Cat# 11835055
Phosphate-buffered saline (PBS) without Ca^{2+} and Mg^{2+}	Thermo Fisher	Cat# 10010049